Materials Research. 2015; 18(6): 1251-1255
DOI: http://dx.doi.org/10.1590/1516-1439.033115

Structural and Magnetic Properties of Hydrothermal Spinel $Ni_{0.4}Zn_{0.6}Fe_2O_4$ Ferrites

Yiwei Zhang[a,b]*, Ailin Xia[a,b], Weihua Chen[c], Renjun Ma[d]

[a]School of Materials Science and Engineering, Anhui University of Technology, Maanshan 243002, China
[b]Anhui Key Laboratory of Metal Materials and Processing, Anhui University of Technology, Maanshan 243002, China
[c]Suining Aviation Station of Civil Aviation Flight, University of China, Suining 629001, China
[d]Anhui Center for Quality Supervision & Test of Casting Products, Hanshan 238100, China

Received: July 30, 2015; Revised: October 18, 2015

Spinel ferrite powder with a nominal composition $Ni_{0.4}Zn_{0.6}Fe_2O_4$ was prepared by a hydrothermal method, following by sintering at 700 °C and 900 °C, respectively. The structural and magnetic properties of specimens are studied. It is found that the large particles in specimens are the agglomerates of many small nanoscale crystallites. A strengthening of chemical polarization of the internal chemical bonds is found in the powder specimen after sintering. The saturation magnetization increases from 50.1 emu/g for as-synthesized powder to 63.1 emu/g for specimen sintered at 900 °C mainly due to the weakening of spin canting, while the coercivity exhibits a slight decreasing variation with the increase of sintering temperature.

Keywords: *soft magnetic material, hydrothermal method, phase composition, microstructure, magnetic properties*

1. Introduction

Spinel (Ni,Zn)Fe_2O_4 (NZFO) ferrite is one of the most extensively studied soft magnetic materials for their fine chemical stability and distinct magnetic and electrical properties[1-5]. Various techniques have been used to synthesize fine NZFO particles with some novel properties compared with corresponding bulks. Gheisari et al.[6] studied the nanocrystalline $Ni_{0.64}Zn_{0.36}Fe_2O_4$ powders by high energy ball milling of ZnO, NiO and Fe_2O_3 powders. Liu et al.[7] prepared nanocrystalline $Ni_{1-x}Zn_xFe_2O_4$ ($0 \leq x \leq 1.0$) powder with grain size of 30 nm using the spraying-coprecipitation method, and the microstructure and magnetic properties of samples after the conventional and microwave sintering were studied. Gabal et al.[8] found that egg-white precursor method provided a simple and cost-effective route to synthesize single phase $Ni_{1-x}Zn_xFe_2O_4$ (x=0.0-1.0) nanopowders. Liu et al.[9] prepared $Ni_{0.5}Zn_{0.5}Fe_2O_4$ nanoparticles by the rapid combustion process and investigated their microstructure and magnetic properties. Gao et al.[10] prepared a series of nanostructured $Ni_{1-x}Zn_xFe_2O_4$ (x=0.0, 0.5 and 1.0) with a grain size from 24 to 65 nm using a sol-gel method, and the effects of composition and sintering temperature on morphology, magnetic properties, Curie temperature, specific heating rate at 295 kHz and hysteresis loss were studied. As a typical chemical method, hydrothermal technique has been used to synthesize NZFO ferrites. Upadhyay has studied the effect of preparation conditions on the formation of nanophase $Ni_{1-x}Zn_xFe_2O_4$ (x=0.0, 0.5 and 1.0) ferrites by chemically precipitating hydroxides followed by hydrothermal processing[11]. Dias & Moreira[12] and Dias et al.[13] studied the sintering process and chemical, mechanical and dielectric properties of $Ni_{0.38}Zn_{0.53}Fe_{2.09}O_4$ powders hydrothermally synthesized by the reaction of an aqueous solution of metal sulfates with NaOH and H_2O_2. However, the magnetic properties of hydrothermal NZFO are seldom reported before, and need further study. In this study, NZFO powder with a nominal composition, $Ni_{0.4}Zn_{0.6}Fe_2O_4$, was hydrothermally synthesized and sintered at different temperatures, and the structural and magnetic properties were studied.

2. Experimental

2.1. Synthesis of specimens

NZFO powders with a nominal composition $Ni_{0.4}Zn_{0.6}Fe_2O_4$ were prepared by hydrothermal method using analytically pure nitrates ($Fe(NO_3)_3$, $Zn(NO_3)_2$ and $Ni(NO_3)_2$) and NaOH as source materials. First, aqueous solutions of nitrates were coprecipitated by NaOH. Then, the precipitates and aqueous solution were hydrothermally reacted in a Teflon liner at 220 °C for 8h. Finally, part of the as-synthesized powder (NZ-P) obtained after hydrothermal process was sintered at 700 °C and 900 °C for 2h, respectively. For convenience, the powders sintered at 700 °C and 900 °C were denoted as NZ-700 and NZ-900, respectively.

2.2. Characterization

Phase identification and microstructural studies were carried out by using X-ray diffractometry (XRD, Rigaku D/max-2550V/PC) with Cu Kα radiation, thermal gravimetric analysis and differential thermal analysis (TGA-DTA, Shimadzu DTG-60(H)), fourier transformed infrared spectrometry

*e-mail: ywzhang14@126.com

(FTIR, Nicolet 6700), scanning electron microscopy (SEM, JEOL JSM-6490LV) and X-ray fluorescence spectrometry (XRF, Arl Advant'x Intellipower 3600). Magnetic hysteresis loops were measured on a vibrating sample magnetometer (VSM, Quantum Design Versalab) with a maximum external field $H_M \approx 1194$ kA·m^{-1} (15000 Oe).

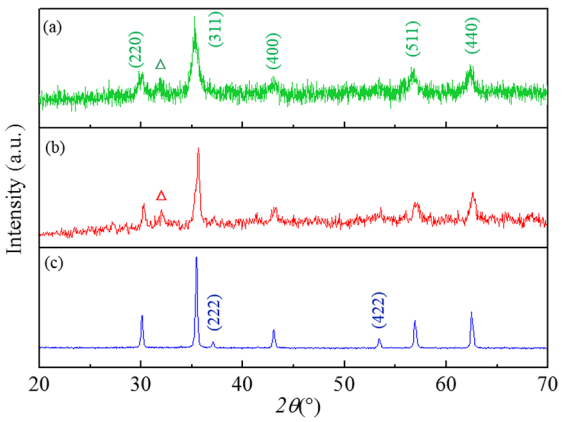

Figure 1. XRD patterns of specimens NZ-P (a), NZ-700 (b) and NZ-900 (c). The marked peak disappeared in (c). A special peak marked by "**Δ**" from specimen in (a) and (b) disappears in (c).

3. Results and Discussion

3.1. Phase identification and microstructural study

Figure 1 shows the XRD patterns of specimens NZ-P, NZ-700 and NZ-900. All the patterns only reveal information of spinel structure (pdf no. 03-0863 for Figure 1a and b, 08-0234 for Figure 1c), which means all the three specimens were single-phase spinel structure. Compared to Figure 1a, the increasingly sharpened peaks in Figure 1b and c indicate the growth of crystallites at high temperatures. According to Scherrer's equation[14], the average crystallite size (D) calculated from Figure 1a-c is 13.7, 19.8 and 38.9 nm, respectively, which increases markedly with the sintering temperatures. Figure 2a-c gives the typical SEM micrographs of specimens NZ-P, NZ-700 and NZ-900, respectively. It is found that some large particles in the micrographs are in the scale of micron meters. Obviously, compared the size of particles in Figure 2a-c with that of crystallites calculated above, regardless whether the powders were sintered or not, the large particles in specimens are the agglomerates of many small nanoscale crystallites. This can be confirmed by Figure 2d which is the detailed SEM micrograph marked in Figure 2b. In fact, generally speaking, the nanoscale crystallites are surely easier to agglomerate extensively. In addition, also found is that the particle size roughly increased with the increase

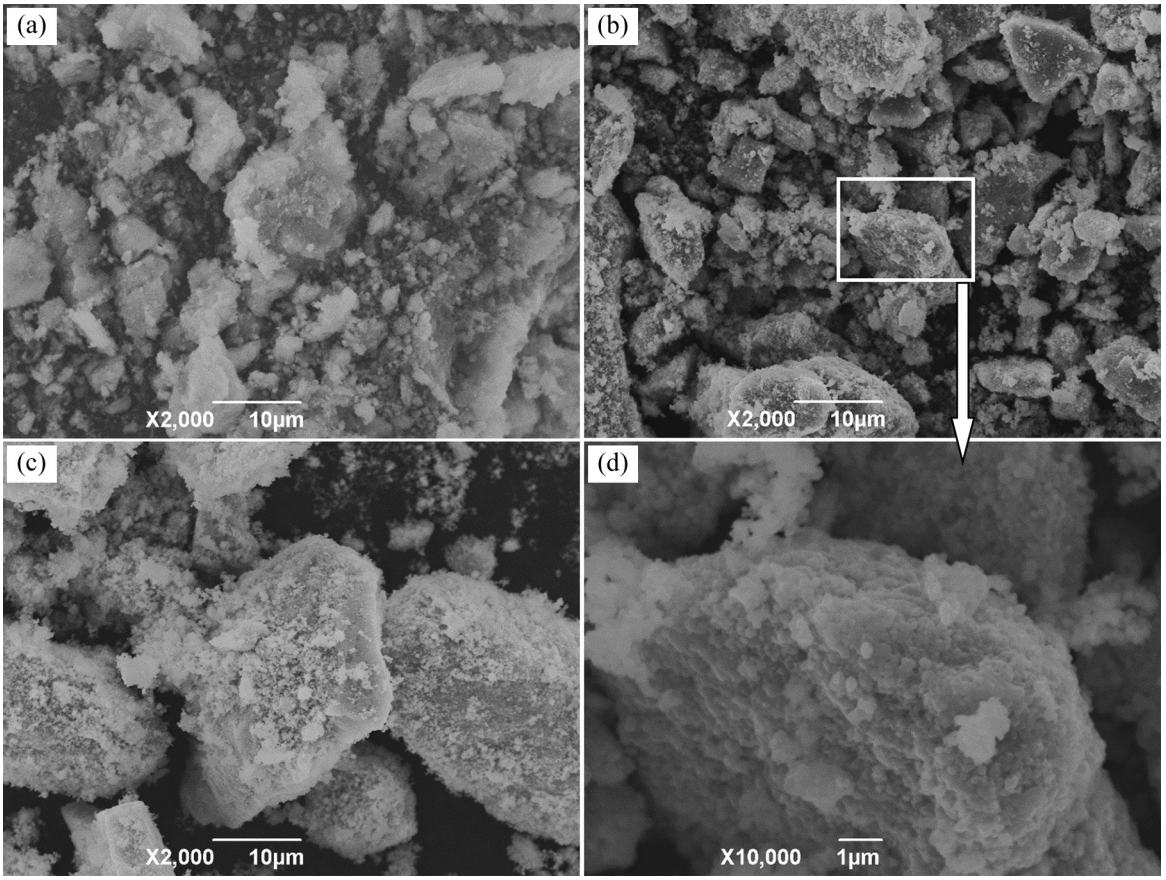

Figure 2. The typical SEM micrographs of specimens NZ-P (a), NZ-700 (b) and NZ-900 (c). (d): the detailed micrograph marked in (b).

of sintering temperatures. Our SEM result is consistent with the previous report[1].

To further interpret the phase composition, XRF, TGA-DTA and FTIR analysis were used to confirm the results of XRD. The nominal and real content (wt%) of metal elements in specimens detected by XRF are listed in Table 1. For either the as-synthesized specimen NZ-P or the sintered specimens NZ-700 and NZ-900, there is only small difference between the real and nominal content, which confirms that the hydrothermal method is very suitable to synthesize magnetic ferrites. Figure 3 gives the TGA-DTA curves (from room temperature to 1000 °C) of specimen NZ-P. The endothermic peak at around 100 °C accompanied with a small weight loss (about 2%) can be attributed to the dehydration of absorbing water in the specimen. What should be elaborated is the very small exothermic peak at around 730 °C, which does not accompany with even a small weight loss. In fact, compared the XRD pattern of NZ-900 with those of NZ-P and NZ-700 in Figure 1, the peak marked by "**Δ**" disappears after sintered at 900 °C, and the 2θ values of other characteristic peaks also change slightly, suggesting a structural change but not phase transition after sintered at 900 °C, which may account for the exothermic peak at around 730 °C. The two endothermic stages from about 400 °C to 650 °C and 750 °C to 1000 °C denoted as stage 1 and 2 in TGA curve, respectively, could be attributed to the growth of crystallites. Seen from the guide dash lines in Figure 3, the slope of stage 1 is clearly smaller than that of stage 2, which indicates the faster growth of crystallite in stage 2. According to the discussion above, the *D* increases slightly from 13.7 to 19.8 nm after sintering at 700 °C, while it increases rapidly to 38.9 nm after sintering at 900 °C, which was consistent with the result of TGA. However, unfortunately, the appearance of exothermic peak at around 200 °C is not elaborated and still need further study.

Figure 4 gives the FTIR spectra of specimens after sintering. From the figure, the characteristic absorption peaks of tetrahedral and octahedral Fe–O stretching band in NZ-700 are at around 583.8 cm^{-1} and 426.7 cm^{-1}[15]. However, after sintered at 900 °C, the corresponding peaks shift slightly to the low wavenumber 579.5 cm^{-1} and 422.2 cm^{-1}, respectively, suggesting a strengthening of chemical polarization of the internal chemical bonds after sintering at higher temperature[16]. Clearly, compared with NZ-700, the structural change in NZ-900 after sintering at 900 °C was confirmed by the FTIR spectra.

3.2. Magnetic properties

Figure 5 gives the magnetic hysteresis loops of specimens NZ-P, NZ-700 and NZ-900, and the corresponding magnetic properties are also listed in Table 2. As is known, for the effects of so-called spin canting in magnetic nanoparticles, the M_S in hydrothermal powder of specimen NZ-P is thought to be lower than that in bulk ferrites[17]. The M_S obtained in NZ-P, NZ-700 and NZ-900 was 50.1, 60.1 and 63.1 emu/g, respectively. Without regard to spin canting, the M_S is an intrinsic parameter affected only by the composition and crystalline structure. According to the results discussed above, the specimens NZ-700 and NZ-900 have the same composition and spinel structure. Therefore, the increase of M_S in sintered

Table 1. The nominal and real content of metal elements detected by XRF in different specimens.

Specimens	Ni	Zn	Fe
NZ-P	10.16	16.03	46.75
NZ-700	10.23	15.92	46.68
NZ-900	10.07	15.72	46.79
nominal	9.85	16.46	46.85

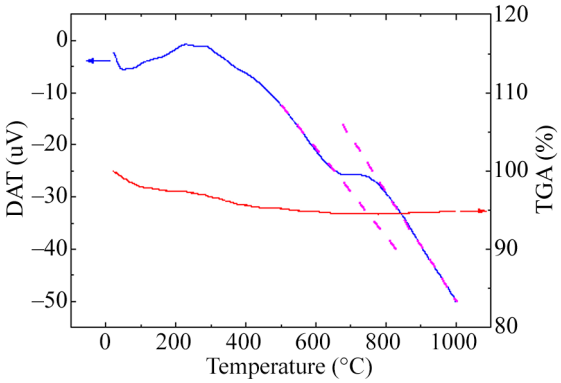

Figure 3. TGA-DTA curves of specimen NZ-P. The dash lines are guide for eyes.

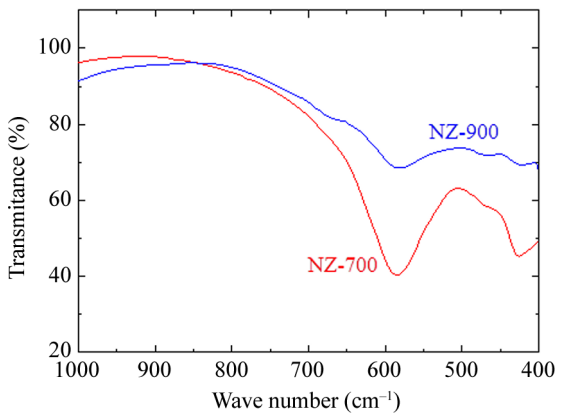

Figure 4. FTIR spectra of specimens NZ-700 and NZ-900.

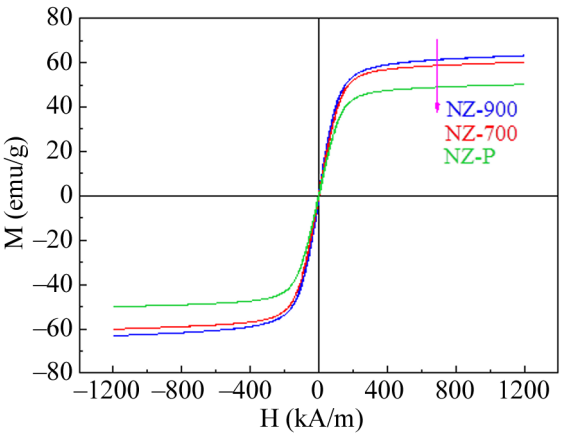

Figure 5. Magnetic hysteresis loops of specimens NZ-P, NZ-700 and NZ-900 at room temperature.

Table 2. The magnetic properties of different specimens.

Specimens	M_S (emu/g)	H_C (kA/m)
NZ-P	50.1	2.70
NZ-700	60.1	2.50
NZ-900	63.1	2.48

specimens can be attributed to the spin canting in magnetic nanoparticles. With the increasing of sintering temperatures, the effect of spin canting became less effective due to the growth of crystallite, which results in the enhancement of M_S in specimen[18]. Of course, the strengthening of chemical polarization of the internal chemical bonds discussed above in NZ-900 is sure to affect its M_S, which is also found in our experimental results of $SrFe_{12}O_{19}$ ferrites[18].

Seen from Figure 5, the ceorcivity (H_C) of specimens NZ-P, NZ-700 and NZ-900 is 2.70, 2.50 and 2.48 kA/m, respectively, which shows a decreasing variation. For ultrafine grains, the H_C behaves proportionally to D^6 as follows[19,20]:

$$H_c = p_c \frac{K_1^4 D^6}{M_s A} \quad (1)$$

where p_C is a dimensionless factor; A is the exchange constant; K_1 is magnetocrystalline anisotropy constant. With the increase of sintering temperatures, the D keeps an increasing variation. Therefore, though the D plays a key role, the decreasing of H_C herein should be ascribed to the effects of K_1 and M_S as well as D.

4. Conclusions

Spinel $Ni_{0.4}Zn_{0.6}Fe_2O_4$ powder was prepared by a hydrothermal method, and then sintered at 700 °C and 900 °C, respectively. According to the structural analysis, a strengthening of chemical polarization of the internal chemical bonds after sintering at 900 °C is found. With the increase of sintering temperatures, the saturation magnetization increases due to the weakening of spin canting, while the coercivity exhibits a decreasing variation.

Acknowledgements

This work was supported by the National Natural Science Foundation of China under Grant No. 11204003.

References

1. Ismail I, Hashim M, Matori KA, Alias R and Hassan J. The transition from paramagnetic to ferromagnetic states as influenced by evolving microstructure of $Ni_{0.5}Zn_{0.5}Fe_2O_4$. *Journal of Superconductivity and Novel Magnetism*. 2012; 25(1):71-77. http://dx.doi.org/10.1007/s10948-011-1201-x.
2. López GP, Condó AM, Urreta SE, Silvetti SP and Aguirre MC. $Ni_{0.5}Zn_{0.5}Fe_2O_4$ nanoparticles dispersed in a SiO_2 matrix synthesized by sol–gel processing. *Materials Characterization*. 2012; 74:17-27. http://dx.doi.org/10.1016/j.matchar.2012.08.010.
3. Shimba K, Tezuka N and Sugimoto S. Magnetic and microwave absorption properties of polymer composites with amorphous Fe-B/Ni–Zn ferrite nanoparticles. *Materials Science and Engineering B*. 2012; 177(2):251-256. http://dx.doi.org/10.1016/j.mseb.2011.12.002.
4. Zhou X-B, Shen L, Li L, Huang T-M, Hu C-F, Pan W-M, et al. Preparation of nanocrystalline-coated carbon nanotube/$Ni_{0.5}Zn_{0.5}Fe_2O_4$ composite with excellent electromagnetic property as microwave absorber. *Journal of Physics D: Applied Physics*. 2013; 46(14):1-6. http://dx.doi.org/10.1088/0022-3727/46/14/145002.
5. Wang ZZ, Wu MZ, Jin SW, Li G, Ma YQ and Wang PH. Ni_3Zn ferrite octahedral nanoparticles with high microwave permeability and high magnetic loss tangent. *Journal of Magnetism and Magnetic Materials*. 2013; 344:101-104. http://dx.doi.org/10.1016/j.jmmm.2013.05.027.
6. Gheisari K, Shahriari S and Javadpour S. Structure and magnetic properties of ball-mill prepared nanocrystalline Ni–Zn ferrite powders at elevated temperatures. *Journal of Alloys and Compounds*. 2013; 552:146-151. http://dx.doi.org/10.1016/j.jallcom.2012.10.036.
7. Liu Y, Yi ZG, Li JJ, Qiu T, Min FF and Zhang MX. Microwave sintering of nanocrystalline $Ni_{1-x}Zn_xFe_2O_4$ ferrite powder and their magnetic properties. *Journal of the American Ceramic Society*. 2013; 96(1):151-156. http://dx.doi.org/10.1111/j.1551-2916.2012.05437.x.
8. Gabal MA, El-Shishtawy RM and Al Angari YM. Structural and magnetic properties of nano-crystalline Ni–Zn ferrites synthesized using egg-white precursor. *Journal of Magnetism and Magnetic Materials*. 2012; 324(14):2258-2264. http://dx.doi.org/10.1016/j.jmmm.2012.02.112.
9. Liu RJ, Shen XQ, Yang XC, Wang QJ and Yang F. Adsorption characteristics of methyl blue onto magnetic $Ni_{0.5}Zn_{0.5}Fe_2O_4$ nanoparticles prepared by the rapid combustion process. *Journal of Nanoparticle Research*. 2013; 15(6):1679-1690. http://dx.doi.org/10.1007/s11051-013-1679-1.
10. Gao P, Hua X, Degirmenci V, Rooney D, Khraisheh M, Pollard R, et al. Structural and magnetic properties of $Ni_{1-x}Zn_xFe_2O_4$ (x=0, 0.5 and 1) nanopowders prepared by sol–gel method. *Journal of Magnetism and Magnetic Materials*. 2013; 348:44-50. http://dx.doi.org/10.1016/j.jmmm.2013.07.060.
11. Upadhyay C, Mishra D, Verma HC, Anand S and Das RP. Effect of preparation conditions on formation of nanophase Ni–Zn ferrites through hydrothermal technique. *Journal of Magnetism and Magnetic Materials*. 2003; 260(1-2):188-194. http://dx.doi.org/10.1016/S0304-8853(02)01320-3.
12. Dias A and Moreira RL. Chemical, mechanical and dielectric properties after sintering of hydrothermal nickel–zinc ferrites. *Materials Letters*. 1999; 39(1):69-76. http://dx.doi.org/10.1016/S0167-577X(98)00219-5.
13. Dias A, Moreira RL and Mohallem NDS. Sintering studies of hydrothermal NiZn ferrites. *Journal of Physics and Chemistry of Solids*. 1997; 58(4):543-549. http://dx.doi.org/10.1016/S0022-3697(96)00162-X.
14. Cao CH, Ren SZ, Zhang LJ and Xia AL. Structural and magnetic properties of spinel (Co,Cu)Fe2O4 ferrites prepared via a hydrothermal and Sintering progress. *Journal of Materials Science Materials in Electronics*. 2014; 25(11):4851-4855. http://dx.doi.org/10.1007/s10854-014-2243-1.
15. Shahane GS, Kumar A, Arora M, Pant RP and Lal K. Synthesis and characterization of Ni–Zn ferrite nanoparticles. *Journal of Magnetism and Magnetic Materials*. 2010; 322(8):1015-1019. http://dx.doi.org/10.1016/j.jmmm.2009.12.006.

16. Xie TP, Xu LJ, Liu CL and Wang Y. Magnetic composite $ZnFe_2O_4$/$SrFe_{12}O_{19}$: preparation, characterization, and photocatalytic activity under visible light. *Applied Surface Science*. 2013; 273:684-691. http://dx.doi.org/10.1016/j.apsusc.2013.02.113.

17. Lu AH, Salabas EL and Schüth F. Magnetic nanoparticles: synthesis, protection, functionalization, and application. *Angewandte Chemie International Edition*. 2007; 46(8):1222-1244. http://dx.doi.org/10.1002/anie.200602866. PMid:17278160.

18. Xia AL, Zuo CH, Zhang LJ, Cao CX, Deng Y, Xu W, et al. Magnetic properties, exchange coupling and novel stripe domains in bulk $SrFe_{12}O_{19}$/$(Ni,Zn)Fe_2O_4$ composites. *Journal of Physics D: Applied Physics*. 2014; 47(41):415004. http://dx.doi.org/10.1088/0022-3727/47/41/415004.

19. Herzer G. Grain size dependence of coercivity and permeability in nanocrystalline ferromagnets. *IEEE Transactions on Magnetics*. 1990; 26(5):1397-1402. http://dx.doi.org/10.1109/20.104389.

20. Xue DS, Chai GZ, Li XL and Fan XL. Effects of grain size distribution on coercivity and permeability of ferromagnets. *Journal of Magnetism and Magnetic Materials*. 2008; 320(8):1541-1543. http://dx.doi.org/10.1016/j.jmmm.2008.01.004.